**IMECE2024-145130**

# METHANE DETECTION AND CHARACTERIZATION WITH AI SENSOR FUSION AND DECISION-ANALYTIC PLACEMENT OF RAPIDLY DEPLOYABLE SENSORS

**Alice M. Agogino[1]\*, Goldstein Adam[2], Ian Yijun Chen[3], Lily Hu[4], Roy Huang[1], Douglas Hutchings[2], Christiana Kang[1], Angeline Ying Kee Lee[1], Yuxin Miao[1], Jeffrey Daniel Millan[1], Vivek Rao[5]**

[1]University of California, Berkeley, CA
[2]Squishy Robotics, Berkeley, CA
[3]Amazon Web Services
[4]Google Research, Google, Mountain View, CA 94043
[5]Duke University

## ABSTRACT

*Immediate action is required to mitigate greenhouse gas emissions and its impact on climate change. Methane emissions have been estimated to produce 80 times the warming effect of carbon dioxide and are responsible for a third of anthropogenic warming. Recent legislation in inspections and penalties for leaks has motivated new efforts to identify sources of fugitive methane emissions and remediate them. However, there are major challenges, costs and safety concerns in identifying and characterizing leaks in remote and hard-to-reach production sites. New international satellite data can be used to flag general areas of large emissions, but do not have the resolution to identify the exact source or faulty equipment, which is needed to develop a plan for remediation.*

*This paper illustrates an integrated ground-aerial smart sensor approach built around a machine learning framework for methane inspections and characterizations. With the ability to be rapidly deployed by sUAS (small unmanned aerial systems) to gather a more localized and ground-level assessment of the leak, a dynamic optimal placement of sensors can be used to for improved remediation decision making. A case study is presented using the methane GasVid leak video dataset.*

**Keywords: Adaptive sampling, mobile sensors, expected value of information, rapid deployment**

## 1. INTRODUCTION

Multiple studies (e.g., United Nations' Intergovernmental Panel on Climate Change [1]), international agreements (e.g., COP26 [2]) and the Federal government (EPA, Inflation Reduction Act [3]) stress the immediate need to find solutions to mitigate climate change. Methane is responsible for up to one-third of the global warming experienced today. Methane traps more heat in the atmosphere per molecule than carbon dioxide, so methane becomes 80 times more harmful than carbon dioxide for 20 years after it is released. The combination of regulatory action, technological advancements, and industry commitment today are driving the market for new innovations.

Measurement of fugitive methane is difficult due to several factors: methane is invisible to the human eye, has no scent, and there are costs and safety issues related to site access. Many production or transmission sites are in unmanned, remote, hard-to-reach locations above tanks or along pipelines. Today, to detect and quantify methane emissions at such locations, human operators often must drive long distances to investigate potential leaks using hand-held sensors. These remote or large-area assessments are costly in terms of personnel-hours, equipment, and safety.

UC Berkeley and Squishy Robotics, Inc. (a spin-off of research on space exploration with NASA that provides rapidly deployable mobile sensing robots for disaster response and remote monitoring [4]) are developing a multimodal system [5] which first detects the general area of methane leaks via satellite data or permanently installed regional sensors and then dynamically hones in on the exact locations of the leak with rapidly deployed sensors to reduce the risk for humans. Our multimodal sensor approach includes range sensing with sensors attached to a drone or permanently installed sensors (e.g, tunable optical gas sensors that detect methane from a distance by mapping voltage values to light absorption at varying gas levels), fused with data from ground-level sensors (e.g., contact gas sensors) that can be dropped by high altitude drones.

In this paper, we describe an AI-decision-analytic framework that is integrated with a methane-specific remotely-controlled sensor robot that can be deployed by drones during periodic inspections or when prompted by a larger area methane survey (such
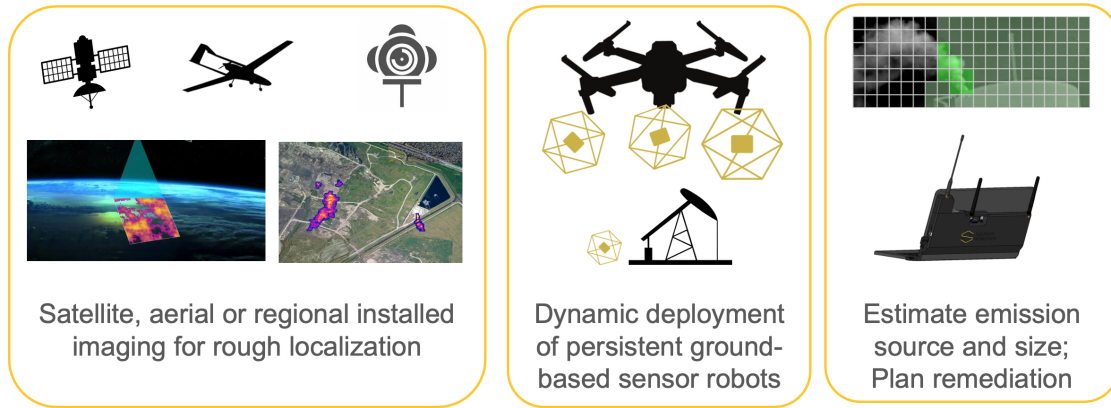
*Corresponding author: agogino@berkeley.edu

**FIGURE 1: Proposed Methane Detection Work Flow.**

as from satellite data [6–8]) that reports a leak present in a general area. This sensor robot will be able to remain on the ground, providing persistent local monitoring over days. It will be able to complement other data from drone-based sensor systems that must fly at a distance due to safety rules and have limited flight time that could cause them to miss intermittent gas leaks. The goal of our multimodal, smart sensor system is to pinpoint the source and size of the methane leak by providing data that can be used for remediation planning, and environmental reporting. The envisioned role of dynamically positioning sensors in a decision-analytic work flow framework for plant monitoring operations, is shown in Fig. 1.

## 2. BACKGROUND AND RELATED WORK

### 2.1 Sources of Methane Leaks in the Oil and Gas Industry

In the United States, agriculture is the largest source of methane emissions, while the second-largest contributor is natural gas and petroleum systems. Methane is released into the atmosphere during various stages, including production, processing, storage, transmission, distribution, and usage of natural gas, as well as production, refining, transportation, and storage of crude oil. Additionally, methane emissions also stem from coal mining. Around 80% of the Oil and Gas sector's methane emissions come from the upstream segment – onshore and offshore oil and gas production. There are three main sources: venting, flaring, and fugitive emissions [9]. This paper focuses on solutions to monitoring fugitive emissions, of which leaky valves, storage tanks or other improperly sealed equipment are the most frequent sources.

### 2.2 Machine Learning for Methane Sensing

Machine learning can be used to improve data analytics over time for enhanced monitoring, diagnostics, and early warning of potential failures. Machine learning can also compensate for limitations in the sensor measurements, response to environmental conditions, and changes in system parameters [10]. Wang et al. [11] [12] collected the first methane leak video dataset - GasVid – with a range of leak types, sizes and imaging distances. They analyzed the data with 2D Convolutional Neural Networks (CNN), 3D CNN and Convolutional Long Short Term Memory (ConvLSTM). They found the 3D CNN to be the most accurate and robust architecture for these data.

We build on the GasVid leak video data set and supplement it with calculated (virtual sensor) data to illustrate the proposed AI-decision-analytic framework in the paper herein. We also apply the innovative Vision Transformer (ViT) [13] model to test its robustness in varying leak conditions and its ability to capture complex patterns in the video data.

### 2.3 Mobile Robots for Industrial Sensing Applications

Mobile sensor robots can address challenges with incomplete sensor coverage or sensor failures with permanently installed sensors [14–16]. Liu et al. [17] provide a review of sensing technologies used in autonomous mobile robots in indoor applications. The role of most of the sensors evaluated are for improved autonomy and not sensing environmental conditions. It compares popular algorithms used in processing these sensor data and technologies of multi-sensor fusion (Kalman filters, particle filters, and neural networks). Wu et al. [18] describe a mobile robotic system for intelligent environmental monitoring with sensors that measure temperature, humidity and airflow velocity. The system outputs the environmental parameters in appropriate displays for better decision making to improve industry environments. Arain et al. [19] propose a mobile robot solution for autonomous gas detection and gas distribution mapping using remote gas sensing. Their "Autonomous Remote Methane Explorer" uses a spectroscopy-based remote gas sensor followed by gas tomography to reconstruct local gas distributions. Their wheeled robot requires a flat surface and needs to be provided with a geometric map of the environment for path planning.

Dynamic sensing has also been implemented in applications using robotic mobile sensing [20–22]. Within mobile sensor platforms, droppable soft robot platforms are particularly advantageous over humans in industrial environments due to their safety and adaptability to a wide range of application areas [4]. Our previous work describes a case study of an industrial work-flow that integrates mobile sensing with machine learning and decision-analytic calculations in the context of the benchmark Tennesssee Eastman data set of a chemical plant [22–25]. Using a plant model with prior and conditional probabilities of failure, Bayesian inference was used to identify the most valuable type and location of physical sensors to be deployed to increase the decision-analytic value of a sensor network [22]. This paper
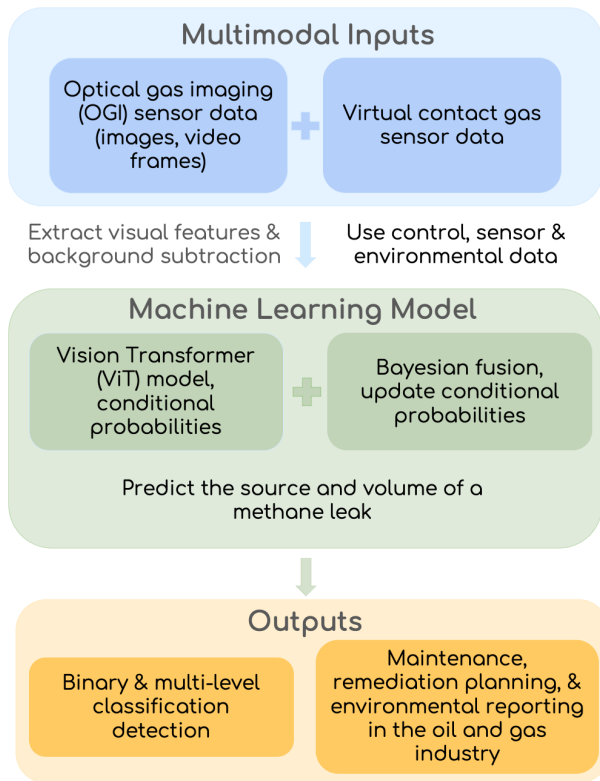
**FIGURE 2: Multimodal Data Pipleline for Machine Learning**

herein builds on this previous work for use for methane detection and remediation planning in the oil and gas industry.

## 3. METHODS AND APPROACH

This section summarizes the opportunities afforded by new rapidly deployable mobile sensor robots and the proposed AI-decision-analytic framework for sensor deployment prioritization. The data set used to illustrate the framework is described along with the methods and approaches used.

### 3.1 Dataset and Data Pipeline

This case study uses the methane GasVid leak video dataset [11], which has about 0.7 million frames of labeled videos of methane leaks from different leaking equipment, covering a wide range of leak sizes and imaging distances. Leak size, defined as the rate at which methane is emitted from the leak source, ranged from 5.3 to 2051.6 gCH4/h. Imaging distances, defined as the distance between the leak source and imaging equipment, ranged from 4.6 to 18.6 meters. Although not seen by the AI models, the location of the leak is at datum 0.0 meter. The data were collected from gas leaks at the METEC (Methane Emissions Technology Evaluation Center) facility at Colorado State University using equipment used at typical oil and gas production sites with gas leak size representative of the majority of leaks in the literature. However, the public data collected focused on an Optical Gas Imager (OGI), which can be thought of as a camera for a narrow wavelength of light associated with methane. Separator videos were recorded at two point-source leak locations – outlet nozzle

tubes on two different pressure vessel separators used for separating a well stream into gaseous and liquid components: separator on pad 1 (13 videos), separator on pad 2 (18 videos). Each represent a different perspective view of a leak. The pad 2 videos were used for training and validation, and the pad 1 videos were used for the testing.

After image processing, a dataset of 591,162 images were used, where the training set and test set were split according to which pad they came from, evenly covering all of the imaging distances used.

The GasVid data set did not include data from low cost gas contact sensors at the same locations taken by the OGI sensors. To simulate the results for deploying other sensors in the same test locations, we developed a virtual sensor to model realistic responses based on the control data and sensor properties in Section 3.4. This is used to illustrate an example for identifying the most valuable type and location of physical sensors to be deployed to increase the decision-analytic value of a sensor network in an oil and gas extraction site application.

A real-time data pipeline using the AWS Cloud Computing Platform was developed to support operations of cloud-based early methane detection through dynamic deployment of sensor robots. The pipeline efficiently manages diverse data types, including sensor readings in JSON format and image data from robots, ensuring robust data ingestion and real-time processing capabilities. An integrated alert system facilitates immediate notifications. A flow chart of the multimodal data pipeline is provided in Figure 2.

### 3.2 AI / Machine Learning Models

In the exploration of machine learning approaches for methane detection and characterization, we evaluated a diverse array of methodologies: 2D CNNs applied to frames extracted from videos, 3D CNNs for video data analysis and sophisticated models like RCNN, ResNet-50, MobileNet. and Vision Transformers (ViT) [13], alongside novel approaches such as Optical Flow and GAN classification.

ResNet-50 is a seminal image recognition model presented in the paper *Deep Residual Learning for Image Recognition* by He et al. [26]. It stood out for its robust performance and capability to handle complex visual data. MobileNet is a class of efficient convolutional models first presented in the paper *MobileNets: Efficient Convolutional Neural Networks for Mobile Vision Applications* by Howard et al. [27]. The MobileNet Model showcased remarkable promise due to its innovative utilization of depth-wise separable convolution and point-wise convolution, enabling significant reductions in computational cost and model size.

We found the Vision Transformer (ViT) model [13] to be most effective for this data set. ViT adapts the transformer architecture, traditionally used in natural language processing, to image recognition tasks. It processes images by dividing them into patches and applying self-attention mechanisms, enabling it to effectively capture complex patterns and dependencies, unlike CNNs that rely on local receptive fields. This approach has allowed ViT to achieve top performance on various image classification benchmarks, challenging the dominance of conventional

CNNs in the field [28].

Our preprocessing strategies were equally diverse, involving background subtraction on video datasets, careful consideration of sample weights to balance data distribution, and down sampling of images to match the resolution of real camera feeds from our sensor configurations.

### 3.3 Expected Value of Information

Fault detection in industrial sensing systems is often performed on sparse data. In such situations, it can be of value to estimate how much the presence of new information may aid in improved situational awareness and the remediation of potential faults. Expected value of information (EVI) is a decision-analytic approach used to ascertain when investment in discovering new information is likely useful and cost-effective, especially in data-sparse situations [29]. EVI depends on the prior distribution of currently-available information, and hence, is formulated as a Bayesian approach [30]. The expected value of sample (or sensor) information (EVSI) is used to determine whether new observations lead to an increase in utility [31]. The expect value of perfect information (EVPI) is the upper limit on any EVSI approach.

In recent years, the use of EVSI to perform efficiency analysis has been widely used in health economics and related fields. It is frequently used to determine optimal sample sizes for randomized clinical trials based on the EVSI of the results of clinical trials [32]. Another common application is in medical research, where EVSI is used to determine whether additional research should be conducted on a topic [33].

EVSI has also been applied to sensing. Maximizing the global EVSI of all data can be used to produce an optimal spatial placement of sensors [15, 34]. Such approaches dynamically add new observations via sequential sampling, at each step choosing the observation corresponding to the largest increase in global EVSI [34, 35].

In this paper, we consider the application of EVSI to the deployment of robotic mobile sensors[20, 21] in methane detection in oil and gas production sites. We define a posterior probability distribution and use EVSI to describe the expected benefit of sensor data collected by a rapidly deployable mobile robot in addition to existing data from a traditional industrial sensing system. Machine learning methods are then utilized to determine the gain in fault detection accuracy, specifically, methane leak detection.

### 3.4 Development of a Virtual Sensor

A virtual sensor calculates critical process conditions using physical sensor readings and mathematical models. They can be useful when a physical sensor is not available in a particular location, but its values can be estimated from other nearby sensors. They can be used to provide redundancy in the system or improve reliability through sensor fusion [36]. A calculated value based on a combination of sensor readings and mathematical models can be used to identify the combination of variables that best characterizes a state. This can be of value in identifying the most effective set of sensors for improving diagnostics at reduced computation [37].

|  | Sensor Predicts Leak | Sensor Predicts Nonleak |
|---|---|---|
| **Leak** | 0.719 | 0.156 |
| **Nonleak** | 0.012 | 0.113 |

**TABLE 1: ViT Binary Confusion Matrix with OGI Sensor Data**

A virtual sensor is used in our case study to illustrate the expected value of new sensor information (EVSI) that can be obtained by rapidly deploying new sensors by aerial vehicles. We modeled the virtual sensor on an inexpensive light-weight LEL sensor typical used to identify volatile gases in emergency response. Its output ranges from 0-100% as a rough measurement of the threshold level to cause an ignition or an explosion. The virtual sensor was calculated from control data, assuming the gas distribution as a Gaussian cone from the leak source and estimating environmental factors from system variables (e.g., gas flow, wind speed and direction).

## 4. RESULTS

### 4.1 Performance Comparison Between Highest Performing ML Models

The accuracy of our leak detection models is defined as the ratio of correctly identified instances to the total number of instances. Application of our MobileNet model achieved an overall test Accuracy of 0.54. The performance varied significantly across the two classes: 0.90 for "Leak" class; 0.10 for "Nonleak" class. MobileNet is designed to be lightweight, which involves a trade-off between accuracy and computational efficiency. This structure design might reduce its ability to capture the full range of features necessary for a balanced performance across diverse classes.

Application of the ViT model produced a much higher overall test Accuracy for the binary case (Leak or no Leak) of 0.832, Recall of 0.822, Precision of 0.984 and F1-Score of 0.895. It's accuracy in predicting leaks, and non-leaks, were 0.822 and 0.905, respectively. Table 1 shows the ViT confusion matrix.

Although the ViT model had relatively high accuracy on the test data as a whole, the set includes six different locations for placement of the OGI sensor relative to the location of the leak (4.6 - 18.6 meters). As can be seen in Table 2, the accuracy goes down as the distance between the leak and sensor increases. As permanently installed OGI sensors are relatively expensive, most remote locations may only have one permanent sensor installed. This sensor would typically be placed at a distance to make sure the majority of the plant is in its field of view. If the OGI sensor, perhaps corroborated with satellite data, indicates that there is a high leak probability, there could be a high value for rapidly deploying another sensor, such as a localized gas sensor, in order verify and find the location of the leak in order to send out the most effective repair team with appropriate parts. The next section explores the expected increase in accuracy with placement of a contact gas sensor.

### 4.2 Improved Accuracy with Contact Gas Sensor

To evaluate the value of adding a new sensor to help with remediation decisions, we derived a virtual sensor (Section 3.4)

| OGI Distance | Overall Accuracy | Leak Accuracy | NonLeak Accuracy |
|---|---|---|---|
| 4.6 | 1.0 | 1.0 | 0.98 |
| 6.9 | 0.98 | 0.98 | 1.00 |
| 9.8 | 0.92 | 0.91 | 0.98 |
| 12.6 | 0.81 | 0.79 | 0.96 |
| 15.6 | 0.77 | 0.75 | 0.97 |
| 18.6 | 0.57 | 0.51 | 0.97 |
| Overall | 0.83 | 0.82 | 0.90 |

**TABLE 2: ViT Binary Accuracy by OGI Sensor Location**

to estimate readings from a virtual contact LEL gas sensor under the control settings used to produce the original GasVid data set, with Gaussian noise added. This contact gas sensor is most accurate when it is in the cloud of the gas release and becomes increasingly less able to detect methane as it is placed away from the cloud.

For purposes of illustration, we assumed all possible leaky valves, containers or other equipment, are located in a line at placements near each of the distances used in Table 2. We use Bayes Theorem to fuse the results of the contact sensor data with those of the original OGI data set.

Taking the Visual Transformer output as sensor $OGI$, the virtual gas contact sensor as sensor $VS$ and the status of the leak as $L$. The conditional probabilities of $P(OGI|L)$ and $P(VS|L)$ can be derived from the relative reliabilities of each sensor. The softmaxed logits from the ViT model were used as $P(OGI|L)$ and the probabilities calculated in *Gasvid Plume models* were used as $P(VS|L)$.

Based on Bayes Theorem and assuming that sensors ($OGI$ and $VS$) are conditionally independent, given the status of $L$, it can be concluded that

$$P(L|FS) = P(L|OGI, VS) = \frac{P(OGI|L)P(VS|L)P(L)}{P(OGI)P(VS)} \quad (1)$$

**NOMENCLATURE**

*Events*
| | |
|---|---|
| $L/\overline{L}$ | Actual Leak/No Leak |
| $OGI/\overline{OGI}$ | Leak/No Leak reading of OGI sensor |
| $VS/\overline{VS}$ | Leak/No Leak reading of virtual sensor |
| $FS/\overline{FS}$ | Leak/No Leak reading of fused sensor |

*Conditional Probabilities*
| | |
|---|---|
| $P(OGI|L)$ | OGI sensor predicts a leak, given a leak |
| $P(FS|L)$ | OGI fusion with virtual sensor predicts a leak, given a leak |

For the given dataset, $P(L) = 7/8$ based on test conditions. In practice, the prior failure probability based on an individual plant location could be used.

## 4.3 Results of Dynamic Sensor Placement and Location Analysis

Independently (as shown in Table 2), ViT achieved an overall accuracy of 0.83 with an accuracy of 0.82 for "Leak" and 0.90 for

| OGI Distance | Fused Sensor Distance | OGI Accuracy | FS Accuracy |
|---|---|---|---|
| 4.6 | 4.6 | 1.0 | 1.0 |
| 4.6 | 6.9 | 1.0 | 0.87 |
| 4.6 | 9.8 | 1.0 | 0.75 |
| 4.6 | 12.6 | 1.0 | 0.75 |
| 4.6 | 15.6 | 1.0 | 0.12 |
| 4.6 | 18.6 | 1.0 | 0.12 |
| 6.9 | 4.6 | 0.98 | 0.98 |
| 6.9 | 6.9 | 0.98 | 0.87 |
| 6.9 | 9.8 | 0.98 | 0.75 |
| 6.9 | 12.6 | 0.98 | 0.75 |
| 6.9 | 15.6 | 0.98 | 0.13 |
| 6.9 | 18.6 | 0.98 | 0.13 |
| 9.8 | 4.6 | 0.91 | 0.95 |
| 9.8 | 6.9 | 0.91 | 0.84 |
| 9.8 | 9.8 | 0.91 | 0.72 |
| 9.8 | 12.6 | 0.91 | 0.72 |
| 9.8 | 15.6 | 0.91 | 0.12 |
| 9.8 | 18.6 | 0.91 | 0.12 |
| 12.6 | 4.6 | 0.79 | 0.93 |
| 12.6 | 6.9 | 0.79 | 0.76 |
| 12.6 | 9.8 | 0.79 | 0.66 |
| 12.6 | 12.6 | 0.79 | 0.67 |
| 12.6 | 15.6 | 0.79 | 0.13 |
| 12.6 | 18.6 | 0.79 | 0.13 |
| 15.6 | 4.6 | 0.75 | 0.90 |
| 15.6 | 6.9 | 0.75 | 0.74 |
| 15.6 | 9.8 | 0.75 | 0.63 |
| 15.6 | 12.6 | 0.75 | 0.64 |
| 15.6 | 15.6 | 0.75 | 0.13 |
| 15.6 | 18.6 | 0.75 | 0.13 |
| 18.6 | 4.6 | 0.51 | 0.89 |
| 18.6 | 6.9 | 0.51 | 0.56 |
| 18.6 | 9.8 | 0.51 | 0.46 |
| 18.6 | 12.6 | 0.51 | 0.47 |
| 18.6 | 15.6 | 0.51 | 0.13 |
| 18.6 | 18.6 | 0.51 | 0.13 |

**TABLE 3: Sensor Fusion with OGI and Virtual Contact Sensor. The Fused Accuracy Should be Interpreted that a Leak is in the Area of the Virtual Sensor (within 5 m)**

"Nonleak" with an OGI sensor. However, when conditioned on the distance the OGI sensor is from the leak the overall accuracy is only 0.57 at 18.6 m, 0.77 at 15.6 m and 0.81 at 12.6 m, not atypical distances when limited to one sensor in a remote location.

Fused with the virtual contact sensor's conditional probabilities derived for each video, the results in Table 3 were obtained. There is information content in the areas that the virtual contact sensor increases or decreases the accuracy relative to that of the OGI sensor by itself. For example, a trend of decreasing accuracy as distance from the leak source increases. This is reasonable as a contact sensor is only accurate when in contact with the methane cloud. However, when fused the data provide not only information about the likelihood of a leak, but also the location of the leak. When coupled with a plant layout, this can greatly assist the remediation strategy in planning the next step.

In the next section, we discuss the implications of a decision-analytical model to recommend optimal sensor placement with an example.

### 4.4 Example AI-Decision-Analytic Scenario

Although an OGI sensor is not expected to find the location or distance to the source of the methane gas, its accuracy diminishes with the distance from the source of a leak (see Table 4). In particular, the true negative probability decreases (0.994 at 4.6 m to 0.222 at 18.6 m) and the false negative probability increases (0.006 at 4.6 m to 0.778 at 18.6 m).

However, a contact gas sensor is designed to sample the air around it and thus has high predictive accuracy near the leak and has low predictive capabilities far from the source. Consider the unfused and fused accuracy shown in Table 3. Regardless of the placement of the OGI sensor, when fused with the virtual contact sensor (creating the fused sensor FS), the fused accuracy has information content on the location of the leak.

For purposes of illustration, let's take the worse-case scenario where the OGI sensor is placed at 18.6 m and the leak is at zero. The conditional probabilities of a leak given that the OGI sensor predicts a leak (true positive) is high at 0.992 as shown in Table 4. When fused with the virtual contact sensor, the true positive rate approaches 1.0 and the false negative approaches 0.0 as shown in shown in Table 5.

If there is a leak, the fused predictions of the leak are highest next to the leak and decrease further away. Thus, in this case, dropping a gas sensor between 4.6 and 18.6 meters, then dropping a second one depending on the results of the first would identify which piece of the equipment has the faculty leak, providing information for planning appropriate remediation. In the next section, we explore dynamic placement of sensors if the expected value of deploying new sensors is greater than the cost of doing so.

### 5. EXPECTED VALUE OF INFORMATION

The Expected Value of Sensor Information (EVSI) is a concept from decision analysis, defined to be the amount a decision maker should be willing to pay for information to reduce or eliminate uncertainty before making critical decisions (see Section 3.3, and is a useful tool for effective management of uncertainty [38] [39] in fault detection in industry. In this study, the value of

| OGI Distance | $P(L\|OGI)$ | $P(L\|\overline{OGI})$ | $P(\overline{L}\|OGI)$ | $P(\overline{L}\|\overline{OGI})$ |
|---|---|---|---|---|
| 4.6 | 0.997 | 0.006 | 0.003 | 0.994 |
| 6.9 | 1.000 | 0.125 | 0.000 | 0.875 |
| 9.8 | 0.997 | 0.385 | 0.003 | 0.615 |
| 12.6 | 0.993 | 0.610 | 0.007 | 0.390 |
| 15.6 | 0.994 | 0.648 | 0.006 | 0.352 |
| 18.6 | 0.992 | 0.778 | 0.008 | 0.222 |

**TABLE 4: Conditional Probability of a Leak Given OGI Sensor Reading by OGI Location (m)**

| Virtual Sensor Distance | $P(L\|FS)$ | $P(L\|\overline{FS})$ | $P(\overline{L}\|FS)$ | $P(\overline{L}\|\overline{FS})$ |
|---|---|---|---|---|
| 4.6 | 1.000 | 0.006 | 0.000 | 0.994 |
| 6.9 | 1.000 | 0.123 | 0.000 | 0.877 |
| 9.8 | 1.000 | 0.272 | 0.000 | 0.728 |
| 12.6 | 1.000 | 0.366 | 0.000 | 0.634 |
| 15.6 | 1.000 | 0.436 | 0.000 | 0.564 |
| 18.6 | 1.000 | 0.473 | 0.000 | 0.527 |

**TABLE 5: Conditional Probability of a Leak Given Fused Sensor Readings with OGI at 18.6 m and Virtual Contact Sensor by Location (m)**

the additional information that sensor fusion with the deployment of a chemical gas (virtual) sensor can provide can be quantified. EVSI calculates the expected improvement in decision making when an additional sensor is added [34]. EVSI has zero value if the information obtained from the new sensor does not change any decisions.

To illustrate the framework in our application on methane leak detection, assume the scenario where satellite data triggers a closer analysis of a production facility for a large methane leak. Assume the cost of sending out a repair crew to be "R" regardless of whether there is a leak or not as the repair crew will still use the time to inspect and test even if there is no leak 6. The cost of a leak includes both the loss of product and added penalties (LC) Fig. 3.

If the OGI reads "leak", the decision is to either deploy the repair team or not is determined by whichever has the lowest expected cost (eq. 2); similarly, if the OGI reads "no leak" (eq. 3) using the prior leak probabilities and the conditional probabilities in Table 4.

$$E_{cost}(OGI) = P(OGI) * \min\left(R, LC * P(L|OGI)\right) \quad (2)$$

| Repair Decision | Ground Truth | Cost |
|---|---|---|
| Repair | Leak | R |
| No Repair | Leak | LC |
| Repair | No Leak | R |
| No Repair | No Leak | 0.0 |

**TABLE 6: Cost table for outcomes of repair decisions, depending on whether a leak has occurred or not**
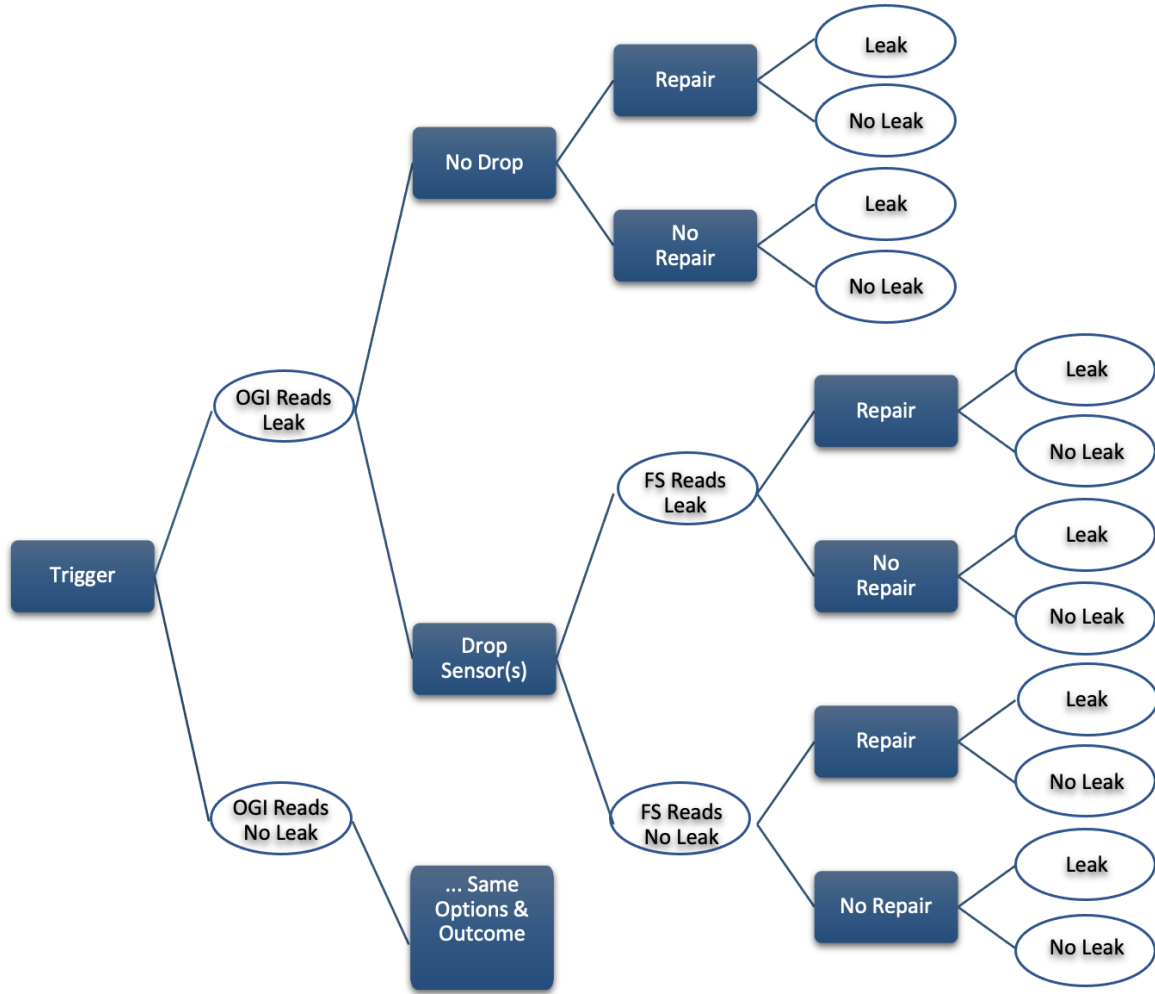
**FIGURE 3: Decision Tree. OGI is the reading of the machine learning outcomes from the OGI video data. FS is the reading of the Fused Sensor.**

$$E_{cost}(\overline{OGI}) = P(\overline{OGI}) * \min\left(R, LC * P(L|\overline{OGI})\right) \quad (3)$$

There is also the option of dropping a chemical gas sensor via drone if the EVSI is positive. The EVSI of adding the sensor will be the difference between the expected cost with the sensor and the expected cost without as shown below (eq. 4) using the conditional probabilities in Table 5. The concept of the expected value of perfect information (EVPI) is value of a perfect sensor with 100% overall accuracy.

$$EVSI = \\ \left[E(\text{cost}_{\text{with no dropped sensors}}) - E(\text{cost}_{\text{with dropped sensors}})\right] \quad (4)$$

Sensors could be dynamically dropped until there is no positive expected value in dropping more.

In this scenario, the optimal decision of sending our a repair crew or not will be highly dependent of the cost of the repair crew,

versus the cost of a leak. Table 7 shows the change in optimal decisions and expected costs as the ratio of $R/LC$ increases from 0.001 to 2.0. If the OGI sensor indicates a leak, the optimal decision is to trust this reading and send out the repair crew as the true leak probability P(L|OGI) is very high (0.92) until the cost of the repair is equal or higher than the cost of a leak ($R/LC \geq$ 1).

However, as the probability of a false negative is high with the OGI sensor at the 18.6 m location, the situation is much different as shown in the last column of Table 7. For the value $R/LC$ =0.001, where the cost of repair is small compared to the cost of a leak, the decision remains the same to repair and not drop a sensor. But for more realistic higher values there is a positive EVSI and the optimal decision is to drop a gas sensor and not repair if "no leak" is confirmed by the chemical sensor.

The corresponding expected outcomes using the fused sensor are show in Table 8. At $R/LC$=0.001, the optimal decision is to "repair" regardless of the sensor reading, as before with the OGI sensor alone. Thus, in this case, with the same decisions there is no value (EVSI=0) in dropping the gas sensor and using the fused

7

data. However, when $R/LC$ is higher, the optimal decision with fused data has changed to recommending "no repair" when FS reads "no leak" until the cost of the repair becomes higher than the cost of the leak. The corresponding EVSI is the difference between the expected costs with the OSI decisions minus the expected costs with the decisions made with the fused data as shown in the last column of Table 8.

How would the results change if the OGI sensor was placed closer to the leak? The decisions are the same when the OGI sensor is at 4.6m but are improved with the fused sensor for all other placements of the OGI sensor with a positive EVSI but with lowering values as the accuracy of the OGI sensor alone increases.

| R/LC | Optimal Decision OGI | Optimal Decision $\overline{\text{OGI}}$ | Expected Cost with OGI Sensor |
|---|---|---|---|
| 0.001 | Repair | Repair | 0.001*LC |
| 0.010 | Repair | Repair | 0.010*LC |
| 0.100 | Repair | Repair | 0.100*LC |
| 0.250 | Repair | Repair | 0.250*LC |
| 0.500 | Repair | Repair | 0.500*LC |
| 0.750 | Repair | Repair | 0.750*LC |
| 1.000 | No Repair | No Repair | 0.875*LC |
| 2.000 | No Repair | No Repair | 0.875*LC |

**TABLE 7: Optimal Decisions with OGI Readings at 18.6 m: With a prior probability of a Leak of 0.875 and the high false negative rate of the OGI sensor at 18.6m from the possible leak, regardless of the OGI Reading (Leak or No Leak), the optimal decision is to play it safe and repair until the cost of a leak (LC) equals the cost of the repair $R/LC$=1.**

| R/LC | Optimal Decision FS | Optimal Decision $\overline{\text{FS}}$ | Expected Cost with FS$Sensor$ | EVSI |
|---|---|---|---|---|
| 0.001 | Repair | Repair | 0.001*LC | 0.000 |
| 0.010 | Repair | No Repair | 0.010*LC | 0.000*LC |
| 0.100 | Repair | No Repair | 0.088*LC | 0.012*LC |
| 0.250 | Repair | No Repair | 0.220*LC | 0.030*LC |
| 0.500 | Repair | No Repair | 0.439*LC | 0.061*LC |
| 0.750 | Repair | No Repair | 0.658*LC | 0.092*LC |
| 1.000 | Equal | No Repair | 0.875*LC | 0.000 |
| 2.000 | No Repair | No Repair | 0.875*LC | 0.000 |

**TABLE 8: Optimal Decisions with Fused Sensor (FS) Readings at 4.6 m: With the satellite data giving a prior probability of a Leak of 0.875, if the FS predicts a leak it will recommend the same decisions as the OGI; the optimal decision is to repair until the cost of a leak (LC) equals the cost of the repair $R/LC$ =1. However, as FS has a higher nonleak accuracy, it only recommends the repair decision for the lowest value of $R/LC$=0.001. The optimal choice at higher values is not to repair. The Expected Value of Sensor Information (EVSI) is the difference between the costs using OGI alone (fourth column of Table 7) and the results in the fourth column of this table.**

| R/L$_l$C | Optimal Decision FS | Optimal Decision $\overline{\text{FS}}$ | Expected Cost with FS Sensor |
|---|---|---|---|
| 0.001 | Repair | Repair | 0.001*$L_l$C |
| 0.010 | Repair | Repair | 0.010*$L_l$C |
| 0.100 | Repair | No Repair | 0.088*$L_l$C |
| 0.250 | Repair | No Repair | 0.095*$L_l$C |
| 0.500 | Repair | No Repair | 0.106*$L_l$C |
| 0.750 | Repair | No Repair | 0.116*$L_l$C |
| 1.000 | No Repair | No Repair | 0.125*$L_l$C |
| 2.000 | No Repair | No Repair | 0.125*$L_l$C |

**TABLE 9: Optimal Decisions with FS Readings for large leaks versus no/small leaks.**

## 6. DISTINGUISHING LARGE LEAKS FROM SMALL LEAKS

In the previous section, we only distinguished between "Leaks" and "No Leaks", regardless of the size of the leak. The Environmental Protection Agency ( EPA) has recently announced new regulations that heavily penalize large methane emitters from the oil and gas industry [3]. This heightens the need to be able to distinguish "Small or No Leaks" from "Large Leaks" that might be subject to these new heavier penalties.

If we consider the previous scenario where the OGI sensor is at 18.6 m and the gas sensor is dropped at 4.6 m and define the Large Leak ($L_l$) category to be 200 ppm or above, the fused accuracy increases to 0.91 compared to 0.89 before mostly because the nonleak accuracy increases. Unfortunately the leak accuracy is lower as the virtual contact sensor has become saturated when only looking at the higher rates. This indicates that a different type of rapidly deployable sensor might be more valuable with leak size is a critical factor.

The different repair decisions and associated expected costs are provided in Table 9. Although the cost ratio appear lower when comparing the expected costs in the fourth column of Table 7 and 8 with those in Table 9, it will depend on the ratio of the original leak cost (L) to the new higher large leak cost ($L_l$C).

## 7. CONCLUSIONS AND FUTURE RESEARCH

In this paper, we used the publicly available methane GasVid leak video dataset [10], which has about 0.7 million frames of labeled videos of methane leaks from different leaking equipment, covering a wide range of leak sizes and imaging distances. The data were collected from controlled experiments at the METEC (Methane Emissions Technology Evaluation Center) facility at Colorado State University. The experiment read OGI sensors from six distances away from a leak (4.6m-18,6m), first with no leak, then at six difference leak volume levels.

We applied multiple machine learning models in leak detection and found that the Vision Transformer model [13], not only achieved top performance with the OGI sensor images, but it also showed improved accuracy when fused with data from a virtual sensor calculated from a simulation of an LEL gas contact sensor using environmental and control variables in the experiment. The virtual sensor was used to simulate the information value of being able to drop new sensors to improve accuracy and

find the location of the leak to make better decisions and plan for appropriate repairs. The accuracy for both the OGI sensor and the virtual sensor decreased with distance from the leak, as would be expected. But the fusion of both increased accuracy when the virtual sensor was in contact with the gas, even for the worse-case when the OGI sensor was at its extreme location of 18.6 m.

Introducing a decision-analytic framework, we calculated the expected costs of using the OGI alone at its worse-case location and the virtual sensor at all locations, assuming it could be dropped at any of them. Using the ratio of repair costs to leak costs ($R/LC$) from 0.0001 to 2.0, we conducted an Expected Value of Information analysis to assess the optimal decisions and expected costs for differing values of $R/LC$. The expected value of information using the fused sensor was positive for most values of $R/LC$, except for extremely small values where it was less expensive to repair or for large values where the cost of a leak was less than a cost of the repair.

There is still much work that can be done in the field of image recognition and classification of methane leaks, given that they are invisible to the human eye and nose. The application of cutting-edge learning models like the Visual Transformer and the ability to rapidly deploy new sensors via drones can greatly increase the accuracy of methane leak predictions and be used to develop more responsive remediation strategies.

Another direction in our research is to better characterize the methane leaks' volume over time. Classification of the size of methane leak has been challenging in the literature [11]. We could improve the accuracy of our virtual sensor by predicting the ideal height for placing the sensor as the methane plume concentration follows a Gaussian distribution with the height. In this paper, we based our virtual sensor on the capabilities of an LEL monitor sensor used to detect hazardous levels of a combustible gas or solvent vapor in air, expressed in % LEL, or Lower Explosive Limit. A 100% LEL is the minimum level that is required to support ignition or combustion. An LEL sensor is used as a safety instrument designed to sound alarms when levels of LEL are above 0%. The LEL level is only a rough indicator of the gas concentration and is not intended to measure the size of the gas leakage. Our goal was to show how an inexpensive "dip stick" sensor could improve accuracy when fused with video images that can't easily distinguish between methane and other clouds, such as water vapor. We intend to develop different virtual sensors to identify the most critical sensor features needed for methane detection and leak size characterization. This could be used to identify which type of sensor would be of the most value for a rapid deployment or permanent installation. It might also shed light on the development of a new generation of sensors with the requisite features.

Future work will also focus on deploying machine learning models on the cloud for advanced image analysis not possible with edge computing on the sensor robot. This enhancement will further improve the system's adaptability and decision-making capabilities in real-time methane detection scenarios.

New laws and regulations in 2024 will greatly increase penalties for large leaks. In 2024, the U.S. Environmental Protection Agency (EPA) published a new rule to implement a "Waste Emissions Charge for Petroleum and Natural Gas Systems" through the Inflation Reduction Act of 2022 (IRA) [3]. This will be a key driver to develop technologies that will reduce the costs and increase human safety associated with measuring methane emissions. The proposed AI-decision-analytic methodology not only improves upon the capabilities of handheld or permanently installed sensor devices but also leverages new satellite data and the capabilities of small unmanned aerial systems (sUAS) capable of deploying small sensor robots.

## REFERENCES

[1] IPCC, 2022. "Climate change 2022: Mitigation of climate change. contribution of working group III to the sixth assessment report of the intergovernmental panel on climate change". Accessed: 2024-05-8, doi=10.1017/9781009157926.

[2] U.S. Department of State, 2024. Cop28. https://www.state.gov/climate-crisis/cop-28/. Accessed: 2024-05-8.

[3] EPA (Environmental Protection Agency), 2024. Inflation reduction act. https://www.epa.gov/inflation-reduction-act. Accessed: 2024-05-8.

[4] Chen, L.-H., Kim, K., Tang, E., Li, K., House, R., Zhu, E. L., Fountain, K., Agogino, A. M., Agogino, A., Sunspiral, V., and Jung, E., 2017. "Soft Spherical Tensegrity Robot Design Using Rod-Centered Actuation and Control". *Journal of Mechanisms and Robotics,* **9**(2), 03.

[5] Squishy-Robotics. Real-time data for swift, nimble, and accurate decision making. https://squishy-robotics.com/. Accessed: 2024-07-14.

[6] NASA/JPL, 2024. Methane source finder: Greenhouse gas mapping. https://methane.jpl.nasa.gov/. Accessed: 7-2024.

[7] EDF, 2024. Methane SAT. https://www.edf.org/methanesat. Accessed: 2024-05-8.

[8] ASI, 2024. Prisma: Hyperspectral satellite, capable of observing from the optical to near infrared. https://www.asi.it/en/earth-science/prisma/. Accessed: 2024-05-8.

[9] EPA, 2023. Estimates of methane emissions by segment in the united states. https://www.epa.gov/natural-gas-star-program/estimates-methane-emissions-segment-united-states. Accessed: 2024-05-8.

[10] Luo, J., Edmunds, R., Rice, F., and Agogino, A., 2018. "Tensegrity robot locomotion under limited sensory inputs via deep reinforcement learning". *2018 IEEE International Conference on Robotics and Automation (ICRA)*, pp. 6260–6267.

[11] Wang, J., Ji, J., Ravikumar, A. P., Savarese, S., and Brandt, A. R., 2022. "Videogasnet: Deep learning for natural gas

methane leak classification using an infrared camera". *Energy,* ***238***, p. 121516.

[12] Wang, J., 2019. "Automating the detection and classification of methane pollution: Integrating deep learning and techno-economic analysis". Phd thesis, Stanford University. Available at https://www.proquest.com/openview/07a9b2d8a2511a33d39a2aa8fa9bd428/1?pq-origsite=gscholar&cbl=18750&diss=y.

[13] Dosovitskiy, A., Beyer, L., Kolesnikov, A., Weissenborn, D., Zhai, X., Unterthiner, T., Dehghani, M., Minderer, M., Heigold, G., Gelly, S., Uszkoreit, J., and Houlsby, N., 2021. "An image is worth 16x16 words: Transformers for image recognition at scale". *arXiv*.

[14] Wang, R., Veloso, M., and Seshan, S., 2016. "Active sensing data collection with autonomous mobile robots". In 2016 IEEE International Conference on Robotics and Automation (ICRA), pp. 2583–2588.

[15] Ballari, D., de Bruin, S., and Bregt, A., 2012. "Value of information and mobility constraints for sampling with mobile sensors". *Computers Geosciences,* ***49***, pp. 102–111.

[16] Schmidt, K., Smith, R. C., Hite, J., Mattingly, J., Azmy, Y., Rajan, D., and Goldhahn, R., 2019. "Sequential optimal positioning of mobile sensors using mutual information". *STATISTICAL ANALYSIS AND DATA MINING*.

[17] Liu, Y., Wang, S., Xie, Y., Xiong, T., and Wu, M., 2024. A review of sensing technologies for indoor autonomous mobile robots. doi.org/10.1177/1740774508098413F.

[18] Wu, J., Huang, Z., Guan, Y., Cai, C., Wang, Q., Xiao, Z., Zheng, Z., Zhang, H., and Zhang, X., 2011. "An intelligent environmental monitoring system based on autonomous mobile robot". In 2011 IEEE International Conference on Robotics and Biomimetics, pp. 138–143.

[19] Arain, M. A., Bennetts, V. H., Schaffernicht, E., and Lilienthal, A. J., 2021. "Sniffing out fugitive methane emissions: autonomous remote gas inspection with a mobile robot". *The International Journal of Robotics Research,* ***40***(4-5), pp. 782–814.

[20] Memarzadeh, M., and Pozzi, M., 2016. "Value of information in sequential decision making: Component inspection, permanent monitoring and system-level scheduling". *Reliab. Eng. Syst. Saf.,* ***154***, pp. 137–151.

[21] Malings, C., and Pozzi, M., 2016. "Value of information for spatially distributed systems: Application to sensor placement". *Reliability Engineering System Safety,* ***154***, pp. 219–233.

[22] Agogino, A., Jang, H. Y., Rao, V., Batra, R., Liao, F., Sood, R., Fang, I., Hu, R. L., Shoichet-Bartus, E., and Matranga, J., 2021. Dynamic placement of rapidly deployable mobile sensor robots using machine learning and expected value of information.

[23] Kulkarni, A., Jayaraman, V. K., and Kulkarni, B. D., 2005. "Knowledge incorporated support vector machines to detect faults in tennessee eastman process". *Computers & chemical engineering,* ***29***(10), pp. 2128–2133.

[24] Khan, A., Ceglarek, D., and Ni, J., 1998. "Sensor Location Optimization for Fault Diagnosis in Multi-Fixture Assembly Systems". *Journal of Manufacturing Science and Engineering,* ***120***(4), 11, pp. 781–792.

[25] Chen, X., 2019. Tennessee eastman simulation dataset.

[26] He, K., Zhang, X., Ren, S., and Sun, J., 2015. Deep residual learning for image recognition.

[27] Howard, A. G., Zhu, M., Chen, B., Kalenichenko, D., Wang, W., Weyand, T., Andreetto, M., and Adam, H., 2017. Mobilenets: Efficient convolutional neural networks for mobile vision applications.

[28] Hwang EE, Chen D, H. Y. J. L. S. J. "Multi-dataset comparison of vision transformers and convolutional neural networks for detecting glaucomatous optic neuropathy from fundus photographs". *Bioengineering (Basel),* ***10***(11).

[29] Hammitt, J. K., and Shlyakhter, A. I., 1999. "The expected value of information and the probability of surprise". *Risk Analysis,* ***19***(1), pp. 135–152.

[30] Choi, Y., Darwiche, A., and den Broeck, G. V., 2017. "Optimal Feature Selection for Decision Robustness in Bayesian Networks". In Proceedings of the Twenty-Sixth International Joint Conference on Artificial Intelligence, IJCAI-17, pp. 1554–1560.

[31] Brennan, A., Kharroubi, S., O'Hagan, A., and Chilcott, J., 2007. "Calculating partial expected value of perfect information via monte carlo sampling algorithms". *Medical Decision Making,* ***27***(4), pp. 448–470. PMID: 17761960.

[32] Willan, A. R., 2008. "Optimal sample size determinations from an industry perspective based on the expected value of information". *Clinical Trials,* ***5***(6), pp. 587–594. PMID: 19029207.

[33] Griffin, S., Welton, N. J., and Claxton, K., 2010. "Exploring the research decision space: The expected value of information for sequential research designs". *Medical Decision Making,* ***30***(2), pp. 155–162. PMID: 20040743.

[34] de Bruin, S., Ballari, D., and Bregt, A., 2012. "Multiphase sensor placement using expected value of information". *International Dairy Journal - INT DAIRY J*, 01.

[35] Chick, S. E., Branke, J., and Schmidt, C., 2010. "Sequential sampling to myopically maximize the expected value of information". *INFORMS Journal on Computing,* ***22***(1), pp. 71–80.

[36] Mattera, C. G., Quevedo, J., Escobet, T., Shaker, H. R., and Jradi, M., 2018. "A method for fault detection and diagnostics in ventilation units using virtual sensors". *Sensors,* ***18***(11).

[37] Vantilborgh, V., Lefebvre, T., Eryilmaz, K., and Crevecoeur, G., 2024. "Data-driven virtual sensing for probabilistic condition monitoring of solenoid valves". *IEEE Transactions on Automation Science and Engineering,* ***21***(2), pp. 1297–1311.

[38] Howard Raiffa, R. S., 1961. *Applied statistical decision theory*. Harvard University Press, Boston, MA.

[39] James C. Felli, G. B. H., 1998. "Sensitivity analysis and the expected value of perfect information". *Medical Decision Making,* ***18***, pp. 95—109.